Mitigating heating of degenerate fermions in a ring-dimple atomic trap

Daniel G. Allman,* Parth Sabharwal, and Kevin C. Wright
Department of Physics and Astronomy, Dartmouth College, 6127 Wilder Laboratory, Hanover, New Hampshire 03766, USA

(Received 5 January 2023; accepted 11 April 2023; published 25 April 2023)

We report on the impact of the extended geometry of a ring-dimple trap on particle-loss heating of a degenerate Fermi gas. When the Fermi level is slightly greater than the depth of the dimple and a broad, low-density "halo" is present, the overall heating rate is reduced relative to the case of a bare ring. We find that the experimentally measured heating rates for the overfilled dimple are in good agreement with a model of the hole-induced heating caused by background-gas collisions. This suppression of the heating rate can be helpful for experimental studies of fermionic superfluids in the weak pairing limit, where achieving and maintaining low temperatures over long timescales are essential.

DOI: 10.1103/PhysRevA.107.043322

I. INTRODUCTION

Experimental studies of fermionic superfluids in the weak-pairing limit require deep quantum degeneracy. However, achieving and maintaining temperatures well below the Fermi temperature in ultracold atomic systems is experimentally challenging. Pauli blocking reduces the efficiency of evaporative cooling in the quantum degenerate regime [1], dramatically slowing down the cooling process (for reviews, see [2,3]). Various protocols have been proposed for circumventing this limitation, relying especially on adiabatic processes with deformations of the trapping potential [4–11]. On top of this fundamental limitation to cooling, deeply degenerate Fermi gases are especially sensitive to losses caused by collisions with background-gas molecules; when atoms deep in the Fermi sea are expelled, the creation of holes substantially raises the effective temperature of the system. This "hole heating" effect was first predicted in Ref. [12] and was previously modeled for uniform and harmonically trapped Fermi gases and Fermi-Bose mixtures [13–15]. These previous studies also investigated the possible use of a bosonic reservoir with a large heat capacity to achieve and maintain low temperatures.

In this paper, we show experimentally that for an inhomogeneous fermionic system with a deeply degenerate subsystem embedded in a large low-density reservoir, the effects of hole heating are reduced compared to the case of a similar system without the reservoir present. This result is achieved by focusing on a ring-dimple trap, a geometry advantageous for studying superfluid phenomena and persistent currents, although we expect the outcome to hold for a generic trapping geometry. More specifically, we investigate the effects of fermion-hole heating for a spin-balanced pair superfluid of ^{6}Li atoms in the deep BCS limit of weak attractive interactions. Minimizing heating rates is important for some experiments with fermion pair superfluids since the natural timescale for investigating low-energy, long-wavelength dynamics in a superfluid ring is set by the period of the lowest quantized circulation state, typically several seconds. It is even more critical for experiments in the deep BCS limit because current methods for detecting supercurrents by matter-wave interference require an interaction ramp to the molecular Bose-Einstein-condensate (BEC) regime before ballistic expansion [16,17]. Unless the initial system temperature is very low, loss of contrast makes coherent phase measurements difficult or impossible. Our most important finding is that the heating rate for fermionic atoms in a superfluid "circuit" can be substantially reduced by embedding it in a large, dilute population of atoms that acts as a heat sink and as a particle reservoir.

This paper is organized as follows: Sec. II gives a brief overview of theory pertaining to noninteracting Fermi systems, along with an outline of the optical potentials employed in the experiment. Section III discusses the *in situ* thermometry technique we used to measure heating rates in the limit of weak attractive interactions. Section IV gives an outline of hole-heating theory and discusses the important findings of our heating-rate measurements. Finally, we conclude in Sec. V by discussing the collisions that reestablish equilibrium throughout the hole-heating process.

II. FERMIONIC ATOMS IN A RING-DIMPLE OPTICAL TRAP

A wide range of magnetic and optical trapping techniques has been used in experiments where BECs of ultracold atoms have been confined to multiply connected trap potentials [18–28]. Experiments with ultracold Fermi gases generally make use of magnetic Feshbach resonances and all-optical trapping techniques, and recent experiments with rings of ultracold fermions have made use of both red- and blue-detuned trap configurations [16,17]. While the conclusions of this paper about heating rates are relevant to a wide range of possible trap configurations, we will focus here on red-detuned ring traps of the type used in our first experiments with rings

*Daniel.G.Allman.GR@Dartmouth.edu

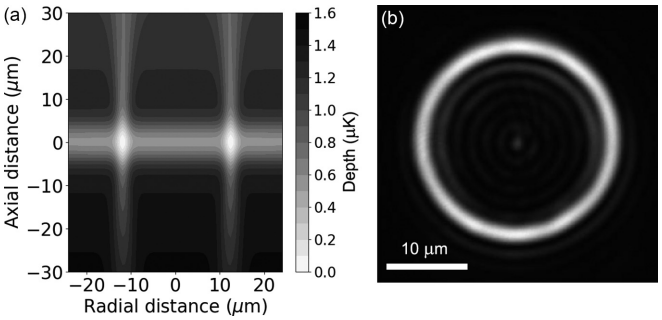

FIG. 1. (a) Side-view cross section of a red-detuned optical trap potential used in our experiments with rings of fermionic atoms. This model includes the effects of the ring beam, the sheet beam, and gravity. (b) Intensity profile of the vertically propagating red-detuned ring-pattern beam modeled in (a).

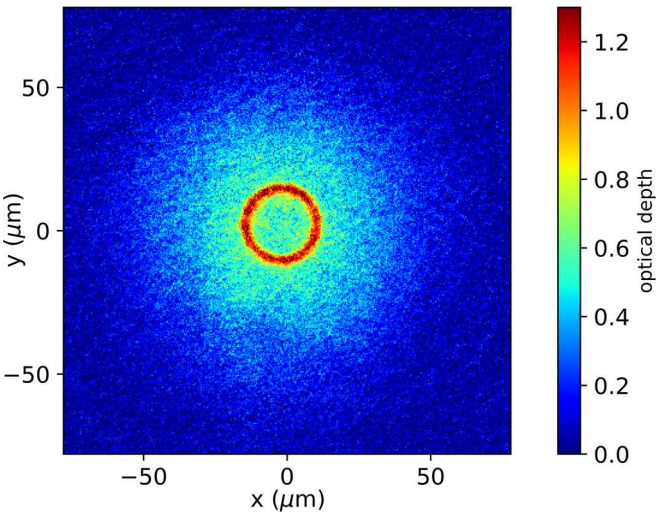

FIG. 2. Density distribution of ^{6}Li atoms in our trap when the Fermi level is around 0.1 μK larger than the depth of the dimple created by the ring-pattern beam. The plot shows the average of 10 *in situ* absorption images taken at a magnetic field of 100 mT. Both the ring-shaped region of increased density and the dilute halo are clearly visible.

of ultracold fermions, which have some potentially helpful features.

Optical ring traps typically employ at least two independent laser fields, one providing mainly vertical confinement and another providing radial confinement. In our experiments with ^{6}Li the main vertical confinement is provided by a red-detuned (1064 nm) horizontally propagating asymmetric Gaussian beam. In most of our experiments, the radial confinement was provided by a red-detuned (780 nm) vertically propagating laser shaped into a ring-pattern beam, as shown in Fig. 1. This overall red-detuned beam configuration is similar to those used in many previous experiments with ring-shaped Bose-Einstein condensates [24]. If the chemical potential of a quantum gas is sufficiently small compared to the depth of the ring dimple, the atoms will be localized to the ring potential minimum, and it is reasonable to treat the transverse confinement as approximately harmonic about the minimum. It is more straightforward to analytically calculate the chemical potential and other important properties of the system when this approximation is valid. For a gas of noninteracting fermionic atoms in a ring with harmonic transverse confinement, the Fermi energy can be expressed as a function of the number of fermions N, the geometric mean of the vertical (z) and radial (r) trapping frequencies $\bar{\omega} = \sqrt{\omega_z \omega_r}$, and the characteristic angular rotation frequency $\Omega \equiv \hbar/(2mr_0^2)$, where r_0 is the ring radius:

$$\frac{E_F}{\hbar\Omega} = \left(\frac{15N}{16}\right)^{2/5} \left(\frac{\bar{\omega}}{\Omega}\right)^{4/5}. \tag{1}$$

We conducted our first experiments expecting to work within this approximation but were surprised to see evidence that heating rates were higher when we evaporated until the Fermi level was smaller than the dimple depth. The atoms in the ring remained in the superfluid phase much longer when the Fermi level was higher, with many atoms spilling from the ring dimple into the shallow extended potential created by the sheet beam, as shown in Fig. 2. This dilute "halo" of atoms typically contained more than two thirds of the total atom population and played a crucial role in the thermodynamics of the system in our experiments. The harmonic approximation is clearly not valid for this situation, so we used a numerical three-dimensional (3D) model of the potential to estimate the relevant thermodynamic properties of our system.

To compute the Fermi energy for atoms in this extended ring-dimple potential, we used a semiclassical model to obtain the total (spin up *and* down) density of states $g_{3D}(E)$ for a fully 3D model of the trap $V(\mathbf{r})$ that included the sheet beam, the ring beam, and gravity:

$$g_{3D}(E) = \frac{8\pi m}{(2\pi\hbar)^3} \int_{V(\mathbf{r})\leqslant E} d^3r \sqrt{2m[E - V(\mathbf{r})]}. \tag{2}$$

We then used the defining relation $N = \int_0^{E_F} g_{3D}(E)dE$ to numerically compute the Fermi energy $E_F(N)$, setting $E = 0$ at the ring-potential minimum. We modeled the ring beam as having an average radius of 12.5 μm and a transverse Gaussian profile with a radial $1/e^2$ half-width of 2.2(1) μm in the plane of the sheet beam. Vertical trapping forces from this tightly focused ring were non-negligible, so we found the through-focus intensity profile by numerically propagating the beam using the angular spectrum method [29] to obtain its full 3D profile. We modeled the sheet beam as having an asymmetric Gaussian profile with a horizontal waist of 290 μm and a vertical waist of 7 μm.

The effect of gravity turned out to be crucial in the numerical calculation of the density of states. While gravity's effect on the exact value of the density of states at a given energy is small, the gradient due to gravity weakens the vertical confinement of atoms more substantially near the ring-dimple region. This is conveniently visualized by plotting vertical cuts of the potential energy at radii near the ring radius $r_0 = 12.5$ μm. These cuts each have a local maximum at some $z < 0$ and linearly fall away to $-\infty$ for $z \ll 0$ due to gravity. The smallest of these maxima lies on the cut along $r = r_0$, as shown in Fig. 3. Its potential energy sets the "evaporation depth" V_{evap} of the trap. Atoms with energy greater than this

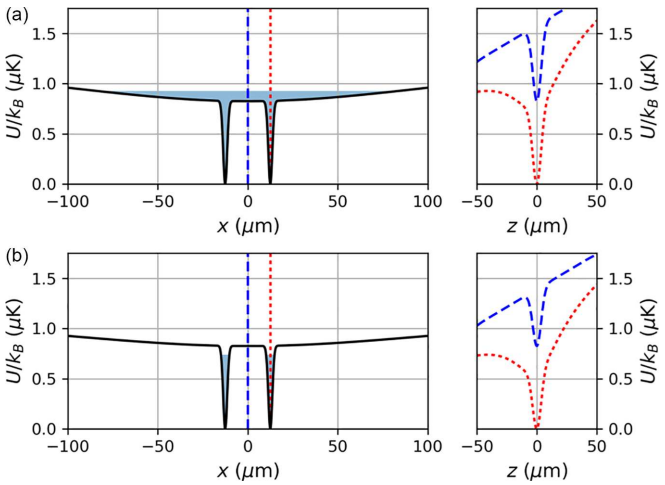

FIG. 3. Potential-energy slices of our combined trap (gravity included) for (a) 40-mW and (b) 30-mW sheet power. The left plots show the radial trap profiles at $z = 0$, while the right plots show the vertical profiles for two different radii: The blue dashed line is the vertical cut along $r = 0$, and the red dotted line is along $r = r_0$. The shaded regions in the radial profiles indicate where the potential energy is below the evaporation depth V_{evap}.

evaporation depth may overcome this "lip" and fall out the bottom of the trap, and thus, states with $E > V_{\text{evap}}$ should carry zero weight insofar as equilibrium thermodynamic quantities are concerned. We therefore multiply Eq. (2) with the step function $\Theta(V_{\text{evap}} - E)$, which in turn has the dramatic effect of placing upper bounds on the allowed atom number and internal energy.

As we will discuss below, there are additional subtleties in addressing states with $E > V_{\text{evap}}$ that may remain bound to the trap via conservation laws that prevent escape through the evaporation channels near the ring dimple. The equilibrium configuration should not include these "quasibound" orbits, but the relaxation dynamics may depend on them.

III. TEMPERATURE MEASUREMENT

We obtained estimates of the system temperature by fitting an appropriate theoretical model to the column density of the halo. In this region, we can approximate the potential $V(r, z) \approx V_{0,s} + m\omega_z^2 z^2/2 + V_{\text{sheet}}(r)$, where $V_{0,s}$ is the potential-energy offset of the full trap at the origin and $V_{\text{sheet}}(r)$ is the cylindrically symmetric sheet potential, with $V_{\text{sheet}}(r = 0) \equiv 0$. To allow for the possibility of mixed dimensionality in our description of the density profile, we quantize the vertical motion to harmonic-oscillator levels while treating the radial motion semiclassically. This procedure is similar in spirit to the theoretical treatment of a quantum well in solid-state systems [30]. In this way, we may write a hybrid description of the density of states:

$$g_j(E) = \frac{s}{(2\pi\hbar)^2} \int d^2r d^2p\, \delta\left(E - \frac{p^2}{2m} - \hbar\omega_z j - V_r(r)\right), \tag{3}$$

which represents the density of available states in the jth axial harmonic-oscillator level ($j = 0, 1, \dots$) for a system with s spin degrees of freedom. We have defined $V_r(r) = V_{0,s} + V_{\text{sheet}}(r) + \hbar\omega_z/2$, accounting for the zero-point energy of the axial motion. Again, we assume states with $E > V_{\text{evap}}$ do not contribute to the density of states. Integrating over momenta and summing over j, we identify the local density of states

$$g(r; E) = s\frac{m}{2\pi\hbar^2}\left\lceil \frac{E - V_r(r)}{\hbar\omega_z} \right\rceil \Theta[E - V_r(r)]\Theta(V_{\text{evap}} - E), \tag{4}$$

where $\lceil x \rceil$ is the ceiling function. The column density $n_2(r)$ is found by integrating the Fermi-Dirac-weighted local density of states over energy, with the substitution $x = E/(k_B T)$, giving

$$\begin{aligned} n_2(r) &= \frac{s}{\lambda_T^2} \int_0^{\eta_c - \frac{q-q(r)}{\gamma}} dx \frac{\lceil x/\gamma \rceil}{e^{x-q(r)} + 1} \\ &= \frac{s}{\lambda_T^2} \sum_{j=0}^{\infty} \left\{ F_0[q(r) - \gamma j] \right. \\ &\quad \left. - F_0\left[q(r) - \gamma j + \frac{q - q(r)}{\gamma} - \eta_c\right] \right\}. \end{aligned} \tag{5}$$

We have further defined $\lambda_T^2 \equiv 2\pi\hbar^2/(mk_B T)$, $\gamma \equiv \hbar\omega_z/(k_B T)$, $q(r) \equiv [\mu - V_r(r)]/(k_B T)$, $\eta_c = V_{\text{evap}}/(\hbar\omega_z)$, and $F_0(x) = \ln(1 + e^x)$ ($\sim e^x$ for $x \to -\infty$). We note, however, that, typically, $\eta_c \gtrsim 20$, so the second term in the summation form of (5) may be neglected, and we will assume this approximation in the subsequent analysis. The integral form of (5) looks remarkably similar to the order-1 Fermi-Dirac integral used to describe the 3D (column) density, except for the presence of the ceiling function in the integrand, which accounts for the discrete axial energy levels. This discreteness is blurred out if either γ or $\gamma/q(r)$ is small compared to unity, which corresponds to the 3D limit. In this case, we can replace $\lceil x/\gamma \rceil$ with x/γ, and the resulting expression gives the proper integrated 3D column density,

$$n_2(r) \approx \frac{s}{\gamma\lambda_T^2} F_1(q(r)), \qquad \gamma \ll 1 \text{ or } \gamma/q(r) \ll 1, \tag{6}$$

where $F_\nu(x)$ is the usual Fermi-Dirac integral of order ν. Conversely, if $\gamma \gg 1$ and $\gamma/q(r) \gg 1$, we approach the two-dimensional (2D) limit, and we may replace $\lceil x/\gamma \rceil$ with 1; the resulting column density gives the proper 2D density,

$$n_2(r) \approx \frac{s}{\lambda_T^2} F_0(q(r)), \qquad \gamma \gg 1 \text{ and } \gamma/q(r) \gg 1. \tag{7}$$

At this point, we have not assumed a particular form for the radially symmetric sheet potential. If we do have knowledge of the sheet trap parameters, however, we may use them to eliminate a fit parameter from the fitting function. In our case, the sheet potential may be described by $V_{\text{sheet}}(r) = V_0[1 - \exp(-2r^2/w_s^2)]$, where $V_0 = m\omega_s^2 w_s^2/4$ and ω_s and w_s are the sheet radial angular trapping frequency and $1/e^2$ radius, respectively. We may therefore introduce $\eta \equiv V_0/(k_B T)$ to write $q(r) = q - \eta[1 - \exp(-2r^2/w_s^2)]$ and eliminate $\gamma = \hbar\omega_z/(k_B T) \equiv \eta/\mathcal{N}$ as a free fit parameter, assuming $\mathcal{N} = V_0/(\hbar\omega_z)$ is a known, albeit potentially uncertain, input. We

rewrite the column density (5) as

$$n_2(r) = n_\infty + n_0 \frac{\sum_{j=0}^{j_{\max}} F_0\left[q - \eta\left(1 - e^{-2\left(\frac{r-r_0}{w_s}\right)^2} + \frac{j}{\mathcal{N}}\right)\right]}{\sum_{j=0}^{j_{\max}} F_0\left(q - \frac{j\eta}{\mathcal{N}}\right)}, \quad (8)$$

where we have introduced n_0 as the column density at $r = r_0$ and allowed for a nonzero density offset n_∞ and center shift r_0 in the density profile. $j_{\max}$ is the number of terms to include in the sum and typically does not need to be very large. In total, there are five free parameters $(q, \eta, n_0, n_\infty, r_0)$ that can be extracted via a least-squares fitting routine. However, one should ensure that n_∞, n_0, and r_0 are as tightly bound and accurate as possible. This is achieved via careful image processing and prefitting analysis of the density profiles. Furthermore, the guesses for the remaining q and η should be physically reasonable. Namely, $\eta \geqslant 0$, and $q = (k_B T/\mu)^{-1}$ must not be too negative when dealing with a presumed nearly degenerate ensemble.

It is also important to note that, for deeply degenerate Fermi gases, absolute temperature enters into the fit of the data only in the far dilute thermal wings of the density distribution. The use of a hybrid fitting function (8) was motivated by this fact, and we found that a simple 3D Fermi-Dirac function consistently overestimated the density at large radii. We found empirically that the largest source of uncertainty in the temperature estimate is from our measurement of the weak radial trap frequency of the sheet beam f_s. Measurement noise introduces a much smaller uncertainty, and uncertainty in the axial trap frequency introduces a similarly small amount. Uncertainty in imaging beam parameters such as saturation intensity and polarization impurity will introduce systematic errors into the temperature estimate. For the dilute-halo atoms, error due to saturation effects may be neglected, and polarization purity is almost unity, so uncertainty related to it may be neglected. Finally, at large radii, the sheet becomes slightly elliptical, and this in turn causes a small systematic shift in measured temperatures to smaller values. This shift becomes more apparent in thermal ensembles in which the extent of the atomic distribution in these elliptical regions is larger.

IV. FERMI-HOLE HEATING

A. Theory

In the far BCS limit, the lifetime of atoms in the trap is limited by the inelastic scattering rate with background particles. In a single background scattering event, a particle in the trap is ejected from the Fermi sea, leaving a hole behind. Assuming the subsequent relaxation dynamics does not eject any additional particles, the temperature increases slightly. For uniform one-body loss with lifetime τ_L, the single-particle populations in state $|k\rangle$ and eigenenergy ϵ_k evolve according to $\dot{n}_k = -n_k/\tau_L$ (k is a set of good single-particle quantum numbers for the inhomogeneous trap). The total atom number $N = \sum_k n_k$ and internal energy $U = \sum_k n_k \epsilon_k$ subsequently evolve as $\dot{N} = -N/\tau_L$ and $\dot{U} = -U/\tau_L$, respectively, where the single-particle loss equation was used. We note that the populations n_k need not be thermally distributed. There are several equivalent methods of deriving the heating rate associated with this loss. Perhaps the most insightful method relies on the observation that the internal energy per particle $u \equiv U/N$ is a conserved quantity. Interestingly, this is true even during the elastic collisions that return the system from a nonequilibrium state to equilibrium after a hole is created. This fact implies that one can, at all times, meaningfully associate an effective temperature to the ensemble as if it were in equilibrium at the same energy and atom number. In our system, the thermodynamic variables used to describe the internal energy per particle u are atom number N, temperature T, and a set of trap parameters which we call $\mathcal{V}$. We note that the *only* thermodynamic role that $\mathcal{V}$ plays is in setting the energy scales for the single-particle energy spectrum, which is fixed for the measurements performed in this paper as we are not varying the trap. The reversible mechanical work associated with trap deformations is therefore set to zero. We thus treat N, U, and T as the only time-varying quantities under one-body loss, with the evolution of $u(t) = u_0$ and $N(t) = N_0 e^{-t/\tau_L}$ known and that of $T(t)$ unknown. We can study the evolution $T(t)$ in a grand-canonical picture, where a time-dependent chemical potential $\mu(t)$ whose role is to fix $N(t)$ at each instant in time is introduced. We thus solve two equations,

$$\frac{U(t)}{N(t)} = u_0 = \frac{\int dE\ g(E) E f[E; \mu(t), T(t)]}{\int dE\ g(E) f[E; \mu(t), T(t)]} \quad (9)$$

and

$$N(t) = N_0 e^{-t/\tau_L} = \int dE\ g(E) f[E; \mu(t), T(t)], \quad (10)$$

for the two unknowns $T(t)$ and $\mu(t)$, where $f(E; \mu, T) = \{\exp[(E - \mu)/k_B T] + 1\}^{-1}$ is the usual Fermi-Dirac distribution function and $g(E)$ is the density of states. By taking a time derivative of (9) and utilizing (10), it is possible to show that the evolution is equivalent to a differential equation governing the temperature dynamics. This is easier to demonstrate, however, by simply differentiating the internal-energy function $U(N, T)$ with respect to time:

$$\dot{U} = \dot{N}(\partial U/\partial N)_T + \dot{T}(\partial U/\partial T)_N. \quad (11)$$

We then use the first law of thermodynamics $dU = TdS + \mu dN = T[dN(\partial S/\partial N)_T + dT(\partial S/\partial T)_N] + \mu dN$ to compute $(\partial U/\partial N)_T = \mu + T(\partial S/\partial N)_T$. Next, the Maxwell relation $(\partial S/\partial N)_T = -(\partial \mu/\partial T)_N$ is used to write $(\partial U/\partial N)_T = \mu - T(\partial \mu/\partial T)_N$. Finally, identifying the heat capacity at constant atom number $C_N = (\partial U/\partial T)_N$, we solve for the temperature derivative in (11):

$$\dot{T} = -\frac{T^2\left(\frac{\partial}{\partial T}\frac{\mu}{T}\right)_N + u_0}{\tau_L c_N}, \quad (12)$$

where $c_N \equiv C_N/N$ and the time-dependent forms for $N(t)$ and $U(t)$ were used. This expression is, in fact, an extension of Eq. (5) in [12], which was derived using energy-balance considerations, to arbitrary temperatures and inhomogeneous traps.

To quantitatively describe the need, in certain experiments, to maintain low temperatures for long times, we briefly draw a connection to the potential experiments performed in the BCS limit, which typically rely on maintaining a temperature below the critical temperature for pairing. Pairing can occur below Gor'kov's critical temperature [31], $k_B T_c \approx 0.277\mu \exp(-\pi\lambda/2)$, with $\lambda = 1/k_F|a|$ being the interaction

parameter. Equating this expression to $k_B T$ gives the threshold reduced temperature above which pairing cannot occur, i.e.,

$$\left(\frac{k_B T}{\mu}\right)_{\max} \equiv 0.277 \exp(-\pi\lambda/2). \tag{13}$$

Even if, initially, $T < T_c$, hole heating will drive the system temperature *and* the critical temperature towards each other until, eventually, $T = T_c$. Using Gor'kov's expression, we write $k_B T(t_c)/\mu(t_c) \equiv 0.277 \exp[-\pi\lambda(t_c)/2]$, defining the time t_c at which the BCS superfluid is completely destroyed and the temperature begins to exceed the critical temperature. We note that t_c depends on the initial interaction parameter $\lambda(t = 0) \equiv \lambda_0$, and that the critical temperature also inherits its time dependence from the one-body loss. Furthermore, we must assume that the BCS pairing gap remains small relative to the Fermi energy to justify the use of the noninteracting model of the hole-heating rate, which will inevitably break down when $\lambda_0 \to 0$.

We emphasize now the role the halo plays in maintaining low temperatures for long periods of time. First, the large density of states offered by the broad sheet helps fermions disperse external energy imparted to the system into the closely spaced energy levels. In other words, the low-density halo has a larger specific heat than the deeply degenerate ring and can serve as an efficient heat sink, lowering the overall heating rate. Second, the halo acts as a particle reservoir for the ring dimple since the global chemical potential is only weakly dependent on the atom number when a substantial halo is present. Intuitively, any atom ejected from the ring dimple can be "replenished" by an atom in the halo. This, in turn, maintains large densities in the ring-dimple region for longer periods of time. Combined, these two effects help maintain a deeply degenerate Fermi gas, especially in the ring-dimple region, for times exceeding the trap lifetime. In comparison, experiments performed in a "bare" ring, i.e., without a halo present, are likely to suffer from unacceptable heating rates. This may become particularly apparent in experiments utilizing a blue-detuned, repulsive ring beam, where the halo population would typically be absent or separated from the superfluid population, unless the potential is carefully tailored to make this possible. Blue-detuned traps have advantageous characteristics for some experiments, but the limits imposed by hole heating will be a much greater problem for experiments requiring many seconds to perform.

The dependence of the heating rate on atom number is, in fact, strongly dependent on the distribution of the fermions in the trap. In particular, the heating rate becomes noticeably suppressed as fermions begin overfilling the ring. We demonstrate this by numerically computing the initial heating rate as a function of atom number using Eq. (12) and the 3D model of the trap density of states. To this end, it is insightful to introduce the "dimple capacity" $N_D \equiv \int_0^{V_{0,r}} g_{3D}(E)dE$, defined as the number of ideal fermion states with energy below the ring depth $V_{0,r}$. In the bare-ring scenario, with $N \leqslant N_D$, the atoms are confined to the ring-shaped region of lowest potential, while for $N > N_D$, atoms spill over into the broad harmonic sheet potential and populate a dilute halo. Figure 4 shows the results of our computations. Figure 4(a) shows

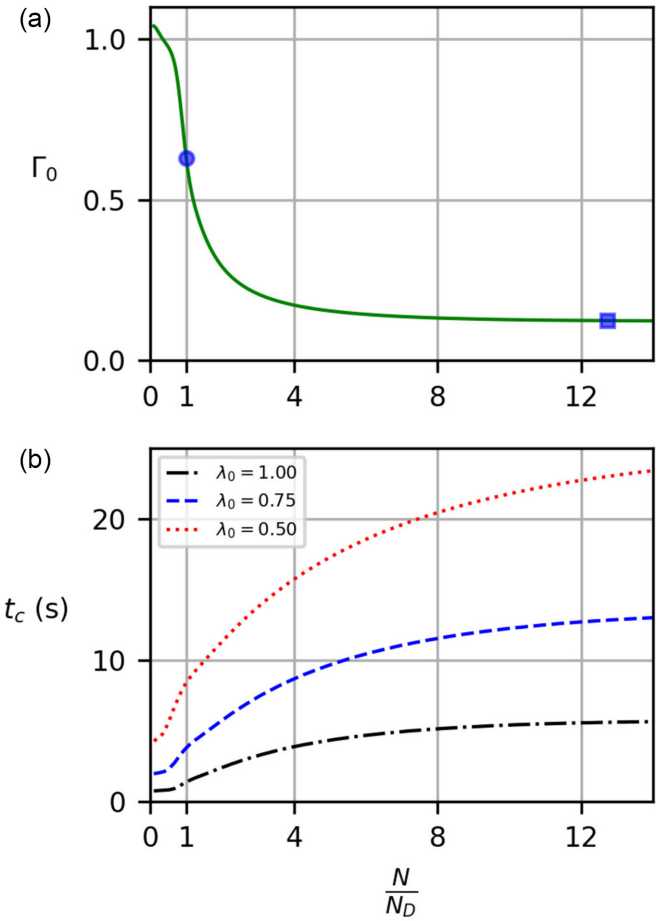

FIG. 4. (a) Predicted initial heating rate (see text) versus atom number relative to the dimple capacity. We show the point where the ring dimple is just filled (blue circle) and the conditions used in the experiment (blue square). (b) Time taken to heat to the critical temperature for different initial values of the interaction parameter λ_0, with $\tau_L = 25$ s. In both plots, $\frac{k_B T}{\mu}|_{t=0} = 0.03$.

the initial dimensionless heating rate $\Gamma_0 \equiv \tau_L \frac{d}{dt}\frac{k_B T}{\mu}|_{t=0}$, where $\frac{k_B T}{\mu}|_{t=0} = 0.03$, as a function of N/N_D. We see a sharp falloff in this rate as the dimple fills up and eventually becomes overfilled, at which point the Fermi energy becomes only weakly dependent on the atom number and the halo becomes populated. For this sheet trap geometry the heating rate approaches a floor of around 0.1 when there are 10 times more atoms in the halo than in the dimple, and there is negligible benefit from increasing the halo population further.

The impact of the reduced heating rate is evident in in Fig. 4(b), which shows the time t_c that it takes for the system to heat from $k_B T/\mu = 0.03$ to the (reduced) critical temperature as a function of the same relative atom number N/N_D and a 25-s vacuum lifetime. The various curves represent different values of the interaction parameter λ_0. The plots for $\lambda_0 > 1$ are not shown because they already begin at $T \gtrsim T_c$. Limits imposed by hole-heating rates clearly become quite restrictive for weakly interacting systems but can be mitigated substantially by allowing the ring to be overfilled.

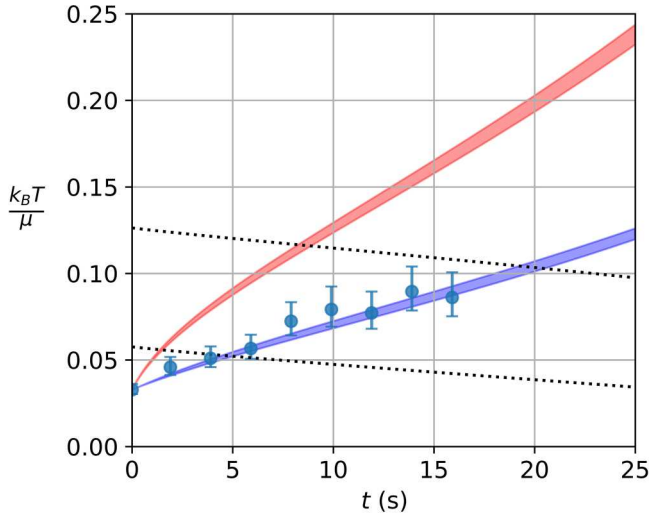

FIG. 5. Reduced temperature versus time for an ideal Fermi gas in our trap potential. Blue circles are experimental data for an overfilled ring dimple with $N = 3.5 \times 10^4$ atoms at $T/T_F = 0.03$. The lower blue filled curve is the temperature predicted by the model described in the text, with $\tau_L = 25$ s and $f_s = 60(4)$ Hz. The upper red filled curve is the model's predicted temperature for $N = 2.7 \times 10^3$ atoms in the same potential, which just barely fills the ring. The black dotted lines show the threshold reduced temperatures $(k_BT/\mu)_{\max}$ required for pairing when $\lambda_0 = 1.0$ (lower) and $\lambda_0 = 0.5$ (upper) in the ring.

B. Experiment

Our experimental apparatus is designed to produce ultracold gases of lithium atoms in highly configurable optical dipole traps. Lithium is a natural choice for these experiments because it has a fermionic isotope (^{6}Li) with high natural abundance, a broad Feshbach resonance, and an unusually stable and long-lived molecular state. After initial cooling and capture using a 2D magneto-optical trap (MOT), 3D MOT, and crossed-beam optical dipole trap, we use a movable optical trap to transport 10^6 atoms to the center of a glass cell located between vertically oriented confocal objective lenses. Magnet coils surrounding the cell can generate a nearly uniform magnetic field of up to 108 mT. We prepare the ^{6}Li atoms in an equal-spin mixture of the two lowest-energy spin states, for which there is a broad Feshbach resonance at 83.2 mT. For more detailed information see the Supplemental Material of Ref. [16].

The typical vacuum-limited lifetime of atoms in our glass cell experimental chamber is at least 1 min. To ensure we could clearly distinguish the effects of hole heating from the effects of slow technical drifts in controlling the experimental conditions, we deliberately reduced the trap lifetime to 25 s by shutting off the ion pumps attached to the 3D MOT vacuum chamber and allowing the pressure in the cell to reach a new equilibrium, pumped only by nonevaporable getters. Under these conditions we evaporatively cooled an initial ensemble of $\sim 10^6$ atoms near the 83.2-mT Feshbach resonance to a final, spin-balanced population of $N = 3.5 \times 10^4$ total atoms. For this number of atoms, the Fermi energy is $E_F = k_B \times 1.1(1)\,\mu$K, computed from the 3D density of states of our numerically modeled trap. The ring and sheet powers were $P_r = 1.3$ mW and $P_s = 50$ mW, respectively. The axial and radial sheet trapping frequencies were measured using a parametric heating technique, and cross-checked using our sheet beam optical model, to be $f_z = 1.6(1)$ kHz and $f_s = 41(2)$ Hz, respectively. Furthermore, our trap model predicts $E_F/V_{\text{evap}} = 0.95$.

Next, to ensure atom loss was predominantly due to one-body background collisions and was not due to rethermalizing collisions (discussed later) or parametric heating via trap vibrations, we recompressed the sheet immediately after evaporation to roughly 2.5 times the minimum sheet power. This, in turn, approximately halved the ratio E_F/V_{evap} and increased the sheet trap frequencies by a factor of $\sqrt{2.5}$. We subsequently ramped the magnetic field adiabatically to 100 mT, where the interaction parameter $1/k_F|a| \approx 1.0$. At this stage, $T/T_F \approx 0.03$. Here, we held the atoms in the trap for varying amounts of time and took a set of absorption images to be used for *in situ* analysis of the local equation of states in the halo region. In particular, we extracted the global reduced temperature k_BT/μ using the hybrid fitting function (8). The use of this hybrid fit function was justified *a posteriori* since the ratio $k_BT/\hbar\omega_z \lesssim 1$ for all hold times used, and dimensional crossover thus occurred in regions of the halo where $\mu(r) \sim \hbar\omega_z$.

Figure 5 shows the reduced temperatures measured in this configuration for different holding times. For comparison, we also plot the predicted temperature profile obtained by numerical integration of the heating-rate equation (12) for the initial conditions, estimated trap parameters, and vacuum lifetime in the experiment. The theory and measurements agree to within the error shown in Fig. 5, which was estimated from temperature fits using the upper and lower bounds of the sheet radial trap frequency, which is the dominant source of uncertainty. The filled region in the theoretical curve is obtained using the same radial sheet frequency uncertainty, which after recompression is about 4 Hz. By comparison, this uncertainty has a much smaller effect on the theoretical heating curve than the experimental one. In Fig. 5 we also show the predicted temperature increase for the bare ring with $N = N_D \approx 2.7 \times 10^3$ atoms in this potential. The effects of hole heating on the system temperature are significantly greater for a bare ring due to the reduced heat capacity per particle. In either case, hole heating also sets a practical limit on the lowest achievable T/T_F due to both the finite state preparation time used in the experiment and the balance between the thermalization rate and hole-heating rate. This window of preparation time is narrower in the bare-ring configuration, however, since the heating rate is roughly twice that of the ring dimple for all hold times shown in Fig. 5.

Additionally, we plot the time-dependent threshold-reduced temperatures, given by the right-hand side of Eq. (13), in Fig. 5 for $\lambda_0 = 1.0$ and $\lambda_0 = 0.5$. t_c can be identified as the time at which the threshold-reduced temperature intersects the reduced-temperature curve. Clearly, a ring-dimple configuration can offer a substantially larger (more than twice as large) window of time to perform BCS-limit experiments compared to a bare-ring configuration. This could be especially important in an experimental apparatus with limited vacuum lifetime or for experiments attempting to probe increasing $1/k_F|a|$ limits.

Because our temperature measurement method involves a fit to the halo atoms, whose broad extent into the harmonic sheet potential makes *in situ* thermometry convenient, we did not obtain measurements of the temperature of atoms in a bare ring, as some other method of thermometry would be required to obtain data for the heating rate in that configuration. One alternative we may eventually employ is to adiabatically deform the trap into a harmonic potential, then relate temperature measurements in that configuration to the temperature of the bare ring by conservation of entropy (see, for example, Refs. [32,33]). This technique is substantially more complex and involves more potential sources of error than extracting the temperature from a fit to the halo, however. The utility that a halo offers for temperature measurements in these kinds of fermionic systems should not be overlooked.

V. THERMALIZATION AND LOSS

In the idealized scenario described above, the equilibrium state after the ejection of an atom by a background collision is still a mostly filled Fermi sea, and subsequent elastic collisions within the system will tend to repopulate the empty state. In the simplest case, this occurs when two atoms at the Fermi level scatter (Pauli blocking suppresses scattering in the Fermi sea); one drops in energy to fill the empty state, and the other is promoted to energy $\epsilon \geqslant E_F$ in something like an Auger process. If $\epsilon \geqslant V_{\text{evap}}$, the excited atom can escape from the trap, and the new equilibrium is a filled Fermi sea with $N-2$ atoms. This loss of an additional atom always occurs (at $T=0$) for $V_{\text{evap}} = E_F$, and the probability decreases to zero when $V_{\text{evap}} = 2E_F$ since the maximum scattering energy is $2E_F$.

More generally, the additional loss above the background rate will depend on other quantities that may include the ratio E_F/V_{evap}, elastic collision rate, temperature, and conserved quantities pertaining to the trap potential. Experimentally, we observed that the initial loss rate was 3 times the background rate when we did not increase the sheet depth after evaporation. This can occur if fermions scattered via the Auger process (with energy up to $2E_F$) scatter off another fermion and in turn excite another fermion to an energy above the Fermi level (up to $1.5E_F$), which can also escape if its energy is above V_{evap}. This process can repeat if one or both of these atoms remain in the trap long enough. Thus, a single background collision in our ring-dimple trap may seed a cascade of energy from a single highly excited "Auger" fermion to a state of many weakly excited fermions above the Fermi level, some of which may escape the trap. A nontrivial trap geometry can make the reequilibration dynamics quite complicated, but qualitatively, we would expect modifications to the loss and heating rates, especially for $E_F \approx V_{\text{evap}}$. In this case the system would typically experience increased initial loss, with high-energy atoms being lost from the trap, keeping the temperature low but causing the Fermi energy to drop rapidly. The loss rate would also become time dependent and asymptotically approach the vacuum-limited loss rate as the Fermi energy drops well below the evaporation depth. These reequilibration dynamics in ring-shaped systems are interesting in their own right, and further experimental and theoretical investigation is warranted.

VI. CONCLUSION

We have demonstrated that one-body loss in a ring-shaped ensemble of ultracold fermions causes heating. We predicted the rate of temperature rise using a model that accounted for hole-induced heating and argued that this heating can be reduced by a particular choice of trap configuration. In particular, maintaining a large, dilute atomic background in contact with the ring helps to dissipate energy imparted into the ensemble via background collisions, which in turn keeps the temperature low for longer periods of time. A high-quality vacuum is still essential to ensure that timescales for heating are long enough to permit low-energy, long-wavelength experiments on superfluids with low critical temperatures, but there are clear advantages to considering forgoing the simplicity of a bare-ring configuration in favor of the more complex, but useful, ring-dimple configuration.

ACKNOWLEDGMENTS

We thank R. Onofrio for insightful discussions and careful reading of the manuscript. This work was supported by the National Science Foundation under Grant No. PHY-2046097.

APPENDIX: LOCAL FERMI ENERGY

It is often insightful to study thermodynamic quantities locally within a local-density-approximation framework. The local Fermi energy, in particular, is a useful energy scale to normalize, e.g., the chemical potential and thermal energy. Again, we would like to account for the possibility of a dimensional crossover in the halo and expect deviations of the true local Fermi energy from its 3D equivalent at low densities. We define the local Fermi energy $E_F(r)$ by integrating (4) as follows:

$$\begin{aligned} n(r) &\equiv \int_{V_r(r)}^{E_F(r)+V_r(r)} g(r;E)dE \\ &= \frac{1}{2\pi a_z^2}\int_0^x dz\lceil z\rceil \\ &= \frac{1}{2\pi a_z^2}[1+2+\cdots+(j_c-1)+j_c\{x\}], \end{aligned} \tag{A1}$$

where $n(r)$ is the column density, $x \equiv E_F(r)/\hbar\omega_z$, $\{x\}$ denotes the fractional part of x, and $a_z^2 \equiv \hbar/(m\omega_z)$. $j_c \equiv \lceil x\rceil$ represents the number of populated axial levels. Note that this definition of the local Fermi energy gives $E_F(r)=0$ for $n(r)=0$, which is conventional. The sum forms a triangle number, and by defining $\tilde{n} = 2\pi a_z^2 n$, we may write (dropping the position label for now)

$$\tilde{n} = j_c(j_c/2 + \{x\} - 1/2). \tag{A2}$$

This equation may be analytically inverted to find the reduced Fermi energy x as a function of the reduced density $\tilde{n}$ as follows. First, we rearrange (A2),

$$\{x\} - 1/2 = \frac{\tilde{n}}{j_c} - \frac{j_c}{2}. \tag{A3}$$

Since the fractional part obeys $0 \leqslant \{x\} \leqslant 1$, the left-hand side is bound between $-1/2$ and $1/2$. Therefore, we seek solutions

j_c that obey $-1/2 \leqslant \frac{\tilde{n}}{j_c} - \frac{j_c}{2} \leqslant 1/2$. Solving for j_c at the end points gives rise to the constraint that

$$\frac{-1+\sqrt{1+8\tilde{n}}}{2} \leqslant j_c \leqslant \frac{1+\sqrt{1+8\tilde{n}}}{2} \tag{A4}$$

for valid solutions to (A3). As j_c is an integer and the region in (A4) has a size of 1 for all $\tilde{n}$, there must be exactly one j_c in that region whose value is simply given by $j_c = \lfloor \frac{1}{2}(1+\sqrt{1+8\tilde{n}}) \rfloor$. Plugging j_c into (A3) and using $x = \lceil x \rceil + \{x\} - 1 = j_c + \{x\} - 1$, the local Fermi energy in this hybrid picture may be written in closed, universal form as

$$\frac{E_F(r)}{\hbar\omega_z} = \frac{\tilde{n}(r)}{\left\lfloor \frac{1}{2}[1+\sqrt{1+8\tilde{n}(r)}] \right\rfloor} + \frac{\left\lfloor \frac{1}{2}[-1+\sqrt{1+8\tilde{n}(r)}] \right\rfloor}{2}. \tag{A5}$$

Figure 6 shows the exact Fermi energy as a function of the 2D density. The Fermi energy reduces to the known results in the 2D ($0 \leqslant \tilde{n} \leqslant 1$) and axially integrated 3D ($\tilde{n} \gg 1$) limits and correctly accounts for the discrete nature of axial harmonic-oscillator levels. It is important to remember that this description holds only *locally* in the halo and does not represent the global Fermi energy of our ring-dimple trap.

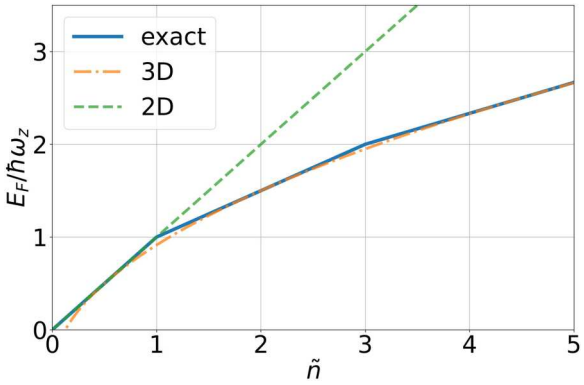

FIG. 6. Reduced Fermi energy as a function of reduced column density, with the 2D ($E_F/\hbar\omega_z \sim \tilde{n}$) and 3D ($E_F/\hbar\omega_z \sim \sqrt{2\tilde{n}} - 1/2$) limiting behaviors shown for comparison. The 2D prediction matches the exact prediction for $\tilde{n} \leqslant 1$.

[1] M. J. Holland, B. DeMarco, and D. S. Jin, Evaporative cooling of a two-component degenerate Fermi gas, Phys. Rev. A **61**, 053610 (2000).

[2] D. C. McKay and B. DeMarco, Cooling in strongly correlated optical lattices: Prospects and challenges, Rep. Prog. Phys. **74**, 054401 (2011).

[3] R. Onofrio, Physics of our days: Cooling and thermometry of atomic Fermi gases, Phys. Usp. **59**, 1129 (2016).

[4] D. M. Stamper-Kurn, H.-J. Miesner, A. P. Chikkatur, S. Inouye, J. Stenger, and W. Ketterle, Reversible Formation of a Bose-Einstein Condensate, Phys. Rev. Lett. **81**, 2194 (1998).

[5] L. Viverit, S. Giorgini, L. P. Pitaevskii, and S. Stringari, Adiabatic compression of a trapped Fermi gas, Phys. Rev. A **63**, 033603 (2001).

[6] P. Schuck and X. Viñas, Suppression of Superfluidity upon Overflow of Trapped Fermions: Quantal and Thomas-Fermi Studies, Phys. Rev. Lett. **107**, 205301 (2011).

[7] G. Zürn, Few-fermion systems in one dimension, Ph.D. thesis, University of Heidelberg, 2012.

[8] S. Stellmer, B. Pasquiou, R. Grimm, and F. Schreck, Laser Cooling to Quantum Degeneracy, Phys. Rev. Lett. **110**, 263003 (2013).

[9] P. M. Duarte, R. A. Hart, T.-L. Yang, X. Liu, T. Paiva, E. Khatami, R. T. Scalettar, N. Trivedi, and R. G. Hulet, Compressibility of a Fermionic Mott Insulator of Ultracold Atoms, Phys. Rev. Lett. **114**, 070403 (2015).

[10] A. Guttridge, A quantum degenerate gas of Cs, in *Photoassociation of Ultracold CsYb Molecules and Determination of Interspecies Scattering Lengths* (Springer, Cham, 2019), pp. 91–111.

[11] L. D. Carr, G. V. Shlyapnikov, and Y. Castin, Achieving a BCS Transition in an Atomic Fermi Gas, Phys. Rev. Lett. **92**, 150404 (2004).

[12] E. Timmermans, Degenerate Fermion Gas Heating by Hole Creation, Phys. Rev. Lett. **87**, 240403 (2001).

[13] L. D. Carr, T. Bourdel, and Y. Castin, Limits of sympathetic cooling of fermions by zero-temperature bosons due to particle losses, Phys. Rev. A **69**, 033603 (2004).

[14] R. Côté, R. Onofrio, and E. Timmermans, Sympathetic cooling route to Bose-Einstein condensate and Fermi-liquid mixtures, Phys. Rev. A **72**, 041605(R) (2005).

[15] Z. Idziaszek, L. Santos, and M. Lewenstein, Sympathetic cooling of trapped fermions by bosons in the presence of particle losses, Europhys. Lett. **70**, 572 (2005).

[16] Y. Cai, D. G. Allman, P. Sabharwal, and K. C. Wright, Persistent Currents in Rings of Ultracold Fermionic Atoms, Phys. Rev. Lett. **128**, 150401 (2022).

[17] G. Del Pace, K. Xhani, A. M. Falconi, M. Fedrizzi, N. Grani, D. H. Rajkov, M. Inguscio, F. Scazza, W. J. Kwon, and G. Roati, Imprinting Persistent Currents in Tunable Fermionic Rings, Phys. Rev. X **12**, 041037 (2022).

[18] S. Gupta, K. W. Murch, K. L. Moore, T. P. Purdy, and D. M. Stamper-Kurn, Bose-Einstein Condensation in a Circular Waveguide, Phys. Rev. Lett. **95**, 143201 (2005).

[19] A. S. Arnold, C. S. Garvie, and E. Riis, Large magnetic storage ring for Bose-Einstein condensates, Phys. Rev. A **73**, 041606(R) (2006).

[20] C. Ryu, M. F. Andersen, P. Cladé, V. Natarajan, K. Helmerson, and W. D. Phillips, Observation of Persistent Flow of a Bose-Einstein Condensate in a Toroidal Trap, Phys. Rev. Lett. **99**, 260401 (2007).

[21] K. Henderson, C. Ryu, C. MacCormick, and M. G. Boshier, Experimental demonstration of painting arbitrary and dynamic potentials for Bose-Einstein condensates, New J. Phys. **11**, 043030 (2009).

[22] G. D. Bruce, J. Mayoh, G. Smirne, L. Torralbo-Campo, and D. Cassettari, A smooth, holographically generated ring trap for the investigation of superfluidity in ultracold atoms, Phys. Scr. **2011**, 014008 (2011).

[23] B. E. Sherlock, M. Gildemeister, E. Owen, E. Nugent, and C. J. Foot, Time-averaged adiabatic ring potential for ultracold atoms, Phys. Rev. A **83**, 043408 (2011).

[24] A. Ramanathan, K. C. Wright, S. R. Muniz, M. Zelan, W. T. Hill, C. J. Lobb, K. Helmerson, W. D. Phillips, and G. K. Campbell, Superflow in a Toroidal Bose-Einstein Condensate: An Atom Circuit with a Tunable Weak Link, Phys. Rev. Lett. **106**, 130401 (2011).

[25] S. Beattie, S. Moulder, R. J. Fletcher, and Z. Hadzibabic, Persistent Currents in Spinor Condensates, Phys. Rev. Lett. **110**, 025301 (2013).

[26] T. W. Neely, A. S. Bradley, E. C. Samson, S. J. Rooney, E. M. Wright, K. J. H. Law, R. Carretero-González, P. G. Kevrekidis, M. J. Davis, and B. P. Anderson, Characteristics of Two-Dimensional Quantum Turbulence in a Compressible Superfluid, Phys. Rev. Lett. **111**, 235301 (2013).

[27] P. Navez, S. Pandey, H. Mas, K. Poulios, T. Fernholz, and W. von Klitzing, Matter-wave interferometers using TAAP rings, New J. Phys. **18**, 075014 (2016).

[28] M. de Goër de Herve, Y. Guo, C. De Rossi, A. Kumar, T. Badr, R. Dubessy, L. Longchambon, and H. Perrin, A versatile ring trap for quantum gases, J. Phys. B **54**, 125302 (2021).

[29] J. W. Goodman, *Introduction to Fourier Optics*, 3rd ed. (Roberts, New York, 2016).

[30] S. Shi, G. Jin, and D. W. Prather, Electromagnetic simulation of quantum well structures, Opt. Express **14**, 2459 (2006).

[31] L. P. Gor'kov and T. K. Melik-Barkhudarov, Contribution to the theory of superfluidity in an imperfect Fermi gas, J. Exptl. Theoret. Phys. (U.S.S.R.) **40**, 1452 (1961) [Sov. Phys. JETP **13**, 1018 (1961)].

[32] C. De Daniloff, M. Tharrault, C. Enesa, C. Salomon, F. Chevy, T. Reimann, and J. Struck, *In Situ* Thermometry of Fermionic Cold-Atom Quantum Wires, Phys. Rev. Lett. **127**, 113602 (2021).

[33] D. Baillie, P. B. Blakie, and A. S. Bradley, Geometric scale invariance as a route to macroscopic degeneracy: Loading a toroidal trap with a Bose or Fermi gas, Phys. Rev. A **82**, 013626 (2010).